

Organic Molecular Compositions and Size Distributions of Chinese Summer and Autumn Aerosols from Nanjing: Characteristic Haze Event Caused by Wheat Straw Burning

GEHUI WANG,^{*,†,‡,§}
 KIMITAKA KAWAMURA,[†] MINGJIE XIE,[§]
 SHUYUAN HU,[§] JUNJI CAO,[†]
 ZHISHENG AN,[†] JOHN G. WASTON,^{†,||}
 AND JUDITH C. CHOW^{†,||}

State Key Laboratory of Loess and Quaternary Geology, Institute of Earth Environment, Chinese Academy of Sciences, Xi'an 710075, China, Institute of Low Temperature Science, Hokkaido University, Sapporo 060-0819, Japan, School of the Environment, State Key Laboratory of Pollution Control and Resources Reuse, Nanjing University, Nanjing 210093, China, and Division of Atmospheric Sciences, Desert Research Institute, Reno, Nevada 89512-1095

Received November 5, 2008. Revised manuscript received June 30, 2009. Accepted July 21, 2009.

Size-segregated aerosol samples were collected in urban Nanjing, China during summer and autumn of 2007 including a period of hazy days during June 1–5. Organic aerosols in the haze event were characterized by elevated concentrations of levoglucosan, high molecular weight (HMW) *n*-alkanes, and HMW fatty acids due to the emissions from field burning of wheat straw. In contrast, organic aerosols on nonhazy days were characterized by a predominance of fossil fuel combustion products. Levoglucosan (4030 ng m⁻³), *n*-alkanes (1520 ng m⁻³), fatty acids (2629 ng m⁻³), and PAHs (57 ng m⁻³) in the haze samples were 3–40 times more abundant than those in nonevent samples. Approximately 30–90% of the organics during the haze period can be attributed to wheat straw burning. Concentrations of particulate material (PM) mass, *n*-alkanes, and low molecular weight (LMW) PAHs showed a unimodal size distribution, peaking at 0.7–1.1 μm during the hazy days, and a bimodal distribution, peaking at 0.7–1.1 μm and 4.7–5.8 μm during nonhazy days. The geometric mean diameters (GMDs) of organic aerosols are larger in the fine mode (<2.1 μm) during the hazy days, suggesting aerosols emitted from the wheat straw burning are larger than those from fossil fuel combustion, and fine particle coagulation and organic compound repartitioning were enhanced.

1. Introduction

Carbonaceous aerosols constitute a substantial fraction of atmospheric particles, and are related to regional and global climate changes (1) and adverse human health effects (2).

* Corresponding author e-mail: wanggh@ieecas.cn; phone: 86-29-8832-9320; fax: 86-29-8832-0456.

[†] Chinese Academy of Sciences.

[‡] Hokkaido University.

[§] Nanjing University.

^{||} Desert Research Institute.

These organic species could modify physical properties of atmospheric particles such as hygroscopicity, albedo, and cloud condensation nuclei activity (3, 4) and chemical properties such as photochemical oxidation activity (5). Local and regional haze occur frequently in many Chinese cities, mainly caused by emissions from vehicle exhausts, coal combustion, biomass burning, and resuspended dust (6, 7). In the farmlands of eastern China such as that near Nanjing (a mega-city), most wheat straw is burned in the field within one week after harvesting (e.g., from the end of May to the beginning of June) in preparation for rice cultivation. Emissions from the biomass burning are transported and mixed with urban pollution, resulting in haze events (8).

To investigate the influence of the biomass burning on urban air quality, size-segregated aerosols were collected during summer and autumn 2007 in urban Nanjing. The sampling periods are classified into haze and nonhaze events to identify differences in the abundances of molecular organic species, and to characterize the size distributions of organic compounds classes.

2. Experimental Section

2.1. Sample Collection. A nine-stage Andersen cascade impactor sampler with prebaked (450 °C, 6 h) quartz fiber filters was set up on the rooftop (10 m above the ground) of a three-story building on the campus of Nanjing University located in the center of the city. The airflow rate was 28 L min⁻¹ with 50% cutoff sizes as >9.0, 9.0–5.8, 5.8–4.7, 4.7–3.3, 3.3–2.1, 2.1–1.1, 1.1–0.7, 0.7–0.4, and <0.4 μm. The sampling was performed during the summer (June 1–17) and autumn (Oct. 12–24) of 2007 each for 4 days. In total, four sets of summer samples and three sets of autumn samples were obtained. The first set of summer samples (June 1–5) coincided with an intensive field burning of wheat straw, classified as a haze event with daily visibilities of 2.6 ± 0.9 km. Meteorological parameters during each of the sampling periods are shown in Table S1.

2.2. Sample Derivatization and GC/MS Analysis. Wang et al. (9) documented the detailed analysis methods for extraction, derivatization, and gas chromatography/mass spectrometer (GC/MS) determination. Briefly, aliquots of the samples and blank filters were ultrasonically extracted with a mixture of dichloromethane and methanol, concentrated to dryness using a rotary evaporation and nitrogen blow-down system, and reacted with *N,O*-bis-(trimethylsilyl)tri-fluoroacetamide.

The derivatized fraction was analyzed using a HP6890-MSD 5973 gas chromatography–mass spectrometer (Agilent Company, USA). The GC separation was carried out on a DB-5MS fused silica capillary column with the GC oven temperature programmed from 50 (2 min) to 120 °C at 15 °C min⁻¹ and then to 300 at 5 °C min⁻¹ with a final isothermal hold at 300 °C for 16 min. The derivatized sample was injected in a splitless mode at an injector temperature of 280 °C and scanned with an electronic impact (EI) mode at 70 eV. GC/MS response factors were determined using authentic standards. Average recoveries of the target compounds were better than 80%. No significant contamination was found in the blanks except for C_{16:0} and C_{18:0} fatty acids, which were less than 2% of those in samples. Data reported here were corrected for the field blanks but not corrected for the recoveries.

3. Results and Discussion

3.1. Differences in the Abundances and Molecular Compositions. Concentrations of organic compounds in each

TABLE 1. Ambient Concentrations^a of Levoglucosan, *n*-Alkanes, Fatty Acids, and PAHs during the Sampling Periods, ng m⁻³

	June 1–5	June 5–9	June 9–13	June 13–17	Oct. 12–16	Oct. 16–20	Oct. 20–24
	haze	nonhaze	nonhaze	nonhaze	nonhaze	nonhaze	nonhaze
I. levoglucosan							
concentration	4030	350	160	103	446	717	929
II. <i>n</i> -alkanes							
C _{m-n} ^b , C _{max} ^c	18–36, 29	18–36, 29	18–36, 29	18–36, 29	18–36, 25	18–36, 25	18–36, 31
∑ <i>n</i> -alkanes	1520	262	258	136	236	412	374
plant wax ^d	1148	94	91	46	39	62	65
fossil fuel ^d	372	168	167	90	197	350	309
WNA% ^e	76	36	35	34	17	15	17
CPI ₁ ^f	7.1	2.0	2.0	1.9	1.4	1.3	1.3
CPI ₂ ^f	2.0	1.2	1.2	1.3	1.3	1.2	1.3
CPI ₃ ^f	12.7	3.5	3.3	3.2	2.0	1.8	1.8
concentration	4030	350	160	103	446	717	929
III. fatty acids							
C _{m-n} ^b , C _{max} ^c	8–32, 28	8–32, 16	8–32, 16	8–32, 16	8–34, 16	8–34, 16	8–34, 16
∑FA	2629	626	515	288	877	1488	1401
FA (≤C _{20:0})	762	384	307	203	492	949	724
FA (>C _{20:0})	1867	242	208	85	385	539	677
CPI ^f	5.0	4.9	4.8	5.4	4.8	4.4	4.4
IV. PAHs							
∑PAHs	57	17	18	22	36	44	38
3&4-ring	12	4	5	5	11	14	11
5&6-ring	36	10	11	13	23	29	26
IP/BghiP	1.0	0.92	1.0	0.91	1.1	0.92	0.97
BghiP/BeP	1.3	1.7	1.1	1.2	0.80	0.73	0.61
total ^g	8236	1255	951	549	1595	2661	2742
PM, μg m ⁻³	318	174	202	172	162	222	294
total ^g /PM, %	2.6	0.7	0.5	0.3	1.0	1.2	0.9

^a Data are the sum of concentrations in all stages. ^b C_{m-n}: homologue concentration ranges. ^c C_{max}: homologue with the maximum concentration. ^d Plant wax *n*-alkanes: calculated as the excess odd homologues–adjacent even homologues average (11) and the difference from the total *n*-alkanes is the fossil fuel-derived amount. ^e WNA%: wax *n*-alkanes percentage, calculated as $\sum C_n - 0.5(C_{n-1} + C_{n+1}) / \sum n\text{-alkanes}$ (25). ^f CPI, carbon preference index, $CPI_1 = \sum \text{odd}(C_{19}-C_{35}) / \sum \text{even}(C_{18}-C_{34})$, $CPI_2 = \sum \text{odd}(C_{19}-C_{27}) / \sum \text{even}(C_{18}-C_{26})$, and $CPI_3 = \sum \text{odd}(C_{27}-C_{35}) / \sum \text{even}(C_{26}-C_{34})$ for *n*-alkanes, $CPI = \sum \text{even}(C_8-C_{32}) / \sum \text{odd}(C_9-C_{33})$ for fatty acids (11). ^g Total: the sum of *n*-alkanes, levoglucosan, fatty acids, and PAHs.

stage were summed and are presented in Table 1 as their ambient concentrations. Aerosol samples collected on June 1-5 showed 3–40 times and 1–9 times higher abundances of levoglucosan (4030 ng m⁻³), *n*-alkanes (1520 ng m⁻³), fatty acids (2629 ng m⁻³) and PAHs (57 ng m⁻³) than those of other summer and autumn samples, respectively (Table 1).

3.1.1. *n*-Alkanes and Levoglucosan. Figure 1a and b show that concentrations of *n*-alkanes (C₁₈–C₃₆) are characterized by one peak at C₂₉ during summer and two peaks at C₂₅ and C₃₁ during autumn, respectively. Such a seasonal difference may be resulted from the enhanced impact of terrestrial plant emissions on the summer samples, especially the sample June 1–5, in which C₂₉ and C₃₁ *n*-alkanes were 10 times more abundant than in other samples (Figures 1a and the inset) (10). Table 1 differentiated total *n*-alkanes into plant wax and fossil fuel emissions (11), and reported carbon preference index (CPI). *n*-Alkanes are commonly associated with terrestrial higher plant origin when CPI > 5 and dominated by fossil fuel combustion when CPI is close to unity (11, 12). As shown in Table 1, for the low molecular weight (LMW) *n*-alkanes (C₁₈–C₂₇), CPI₂ was 2.0 in the haze event sample and 1.2–1.3 in all other samples. For the high molecular weight (HMW) *n*-alkanes (C₂₆–C₃₅), CPI₃ was 12.7 in the haze event sample and 1.8–3.5 in other samples. The elevated CPI of the June 1–5 sample confirmed the abundances of terrestrial plant wax, which accounted for 76% of total *n*-alkanes.

Levoglucosan varied by 40 fold between haze (4030 ng m⁻³ on June 1–5, Table 1) and nonhaze events (103–350 ng m⁻³ on June 5–17 and 446–929 ng m⁻³ on Oct. 12–24). Lipids of wheat straw are abundant with HMW *n*-alkanes (C₂₉ and C₃₁) and fatty acids (C_{24:0}, C_{28:0}, and C_{30:0}) (13), and levoglu-

cosan is a tracer for biomass burning smoke (11). Therefore, the sharply enhanced concentrations of HMW *n*-alkanes and levoglucosan in the sample June 1–5 clearly demonstrated that the haze event on June 1–5 was mainly caused by the field burning of wheat straw, the emissions of which were transported into the urban area and accumulated within the boundary layer with urban pollutants, leading to the very poor visibility (2.6 km on average, Table S1).

Table 1 showed that CPI values (e.g., 1.9–2.0 for CPI₁) and wax *n*-alkane content (WNA%, 34–36%) for the three samples collected during June 5–17 were similar. Although similar molecular compositions were also observed for the three autumn samples (Oct. 12–24), the abundances of *n*-alkanes varied by two folds. These low values of CPI and WNA% samples are grouped as nonhaze event. Averages of each of the three samples for summer (June 5–17) and autumn (Oct. 12–24) periods were used for further analyses.

3.1.2. Fatty Acids and PAHs. Fatty acids (FAs) in the range of C_{8:0}–C_{34:0} were found from the nonhaze event samples with major and minor C_{max} at C_{16:0}/C_{18:0} and C_{24:0}/C_{28:0}, respectively. Figure 1c and d showed the predominance of even carbon number (CPI: 4.4–5.4 for C_{8:0}–C_{32:0}, Table 1), consistent with the findings of Wang et al. (9). However, the haze event sample (i.e., the June 1–5 sample in Figure 1c) showed a different molecular distribution, in which C_{28:0} was much higher than C_{16:0}. LMW FAs (≤C_{20:0}) have multiple sources and thus only indicate a biogenic input, while HMW FAs (>C_{20:0}) originate from terrestrial plant wax (11). Concentrations of HMW FAs in the haze event sample were 8–15 times higher than those in the summer nonhaze event samples compared to 2–3 times abundances of LMW FAs in the haze event sample (Table 1). Because HMW FAs are

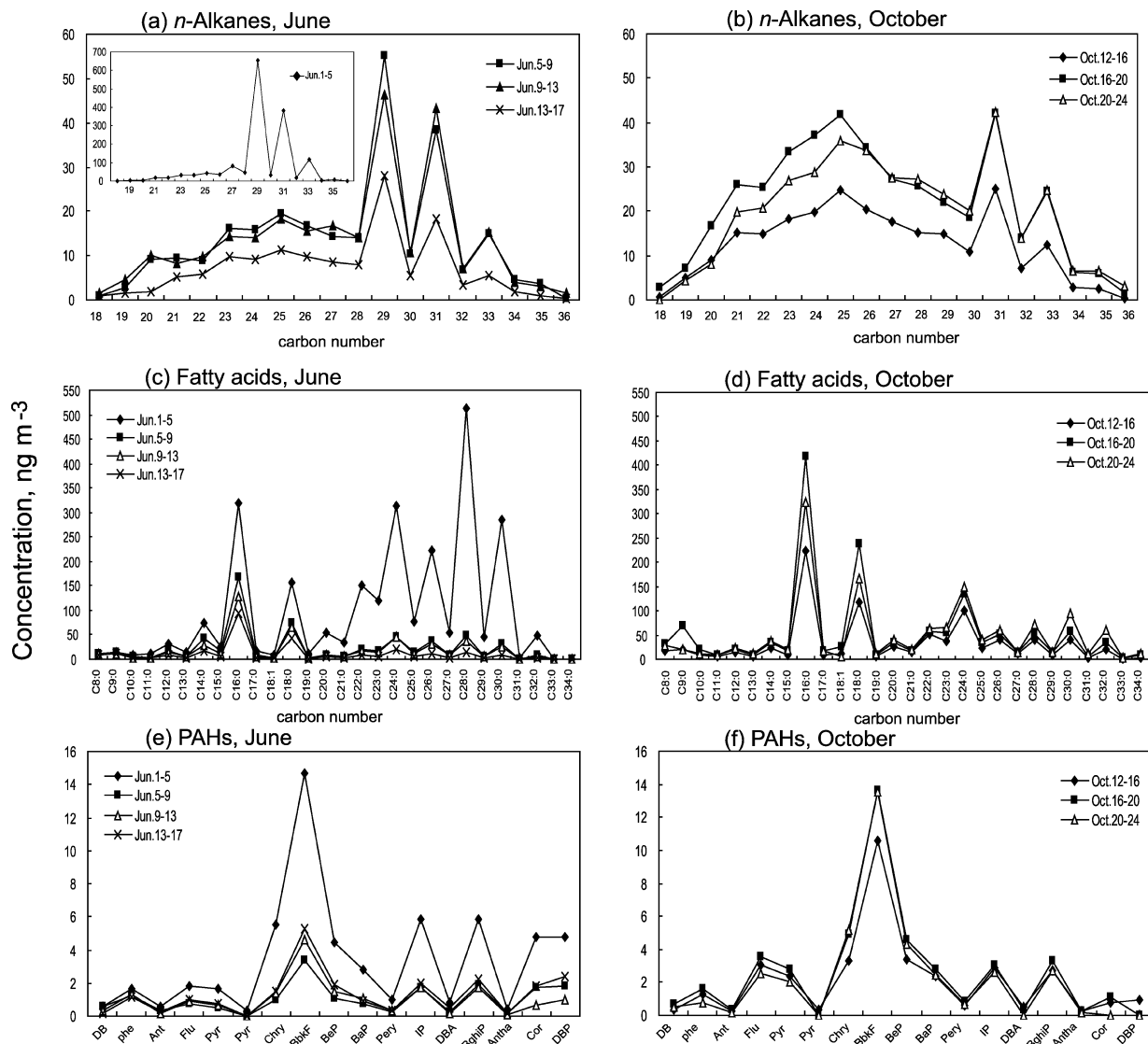


FIGURE 1. Differences in the molecular compositions of particulate matter (PM)-associated (a, b) *n*-alkanes, (c, d) fatty acids, and (e, f) PAHs in June and October (Abbreviation of PAHs: dibenzothiophene, DB; phenanthrene, Phe; anthracene, Ant; fluoranthene, Flu; pyrene, Pyr; chrysene, Chry; benzo(b/k)fluoranthene, BbkF; benzo(e)pyrene, BeP; benzo(a)pyrene, BaP; perylene, Pery; indeno(1,2,3-cd)pyrene, IP; dibenz(a,h)anthracene, DBA; benzo(ghi)perylene, BghiP; anthanthrene, Antha; coronene, Cor; dibenzo(a,h)pyrene, DBP).

abundant in plant wax of wheat straw (13), such high levels of HMW FAs in the June 1–5 sample again confirmed the significant impact due to the field burning of wheat straw.

As shown in Figure 1e and f, seventeen PAHs were determined, with benzo(b/k)fluoranthene (BbkF) being most abundant, followed by indeno(1,2,3-cd)pyrene (IP) and benzo(ghi)perylene (BghiP). PAHs concentration (57 ng m⁻³, Table 1) in the haze event sample was 1–3 times higher than those (17–44 ng m⁻³) in the nonhaze event sample. Concentration ratios of PAHs are indicative of specific sources. For example, IP/BghiP mass ratios in emissions from gasoline, diesel, and coal are 0.2, 0.5, and 1.3 (14), and benzo(ghi)perylene/benzo(e)pyrene (BghiP/BeP) in vehicle exhaust and coal burning smoke are 2.0 and 0.8 (15). As shown in Table 1, summertime ratios of IP/BghiP and BghiP/BeP between the haze and nonhaze samples were similar, whereas BghiP/BeP ratios were slightly lower for the autumn nonhaze samples, suggesting a slight difference in PAH sources between the two seasons.

Abundances of *n*-alkanes, FAs, PAHs, and levoglucosan in fine mode (<2.1 μm) relative to those in coarse mode (≥2.1 μm) are shown in Figure 1S. Fine fractions of all the

organic compound classes significantly increased in the June 1–5 sample but the averaged values for June 5–17 and Oct. 12–24 were rather similar to each other. Based on the concentrations and molecular compositions of the organic compounds discussed above, we concluded that the aerosol compositions and concentrations of the June 1–5 sample, the haze event sample, are characterized by the products from field burning of wheat straw, while the aerosol samples collected on June 5–17 and Oct. 12–24, the nonhaze event samples, are characteristic of fossil fuel combustion products.

3.2. Size Distributions. Differences in the size distributions of the major organic species among the haze and nonhaze samples are shown in Figures 2–4. Geometric mean diameters (GMD) of the organic aerosols in the fine (<2.1 μm) and coarse (≥2.1 μm) fractions are shown in Table 2 (16, 17).

3.2.1. PM Mass, Levoglucosan, and *n*-Alkanes. For the June 1–5 sample, particle concentrations were 50% higher in the fine fraction than in the coarse fraction peaking at 0.7–1.1 μm size (Figure 2a). Particle concentrations for the nonhaze samples showed similar bimodal distributions

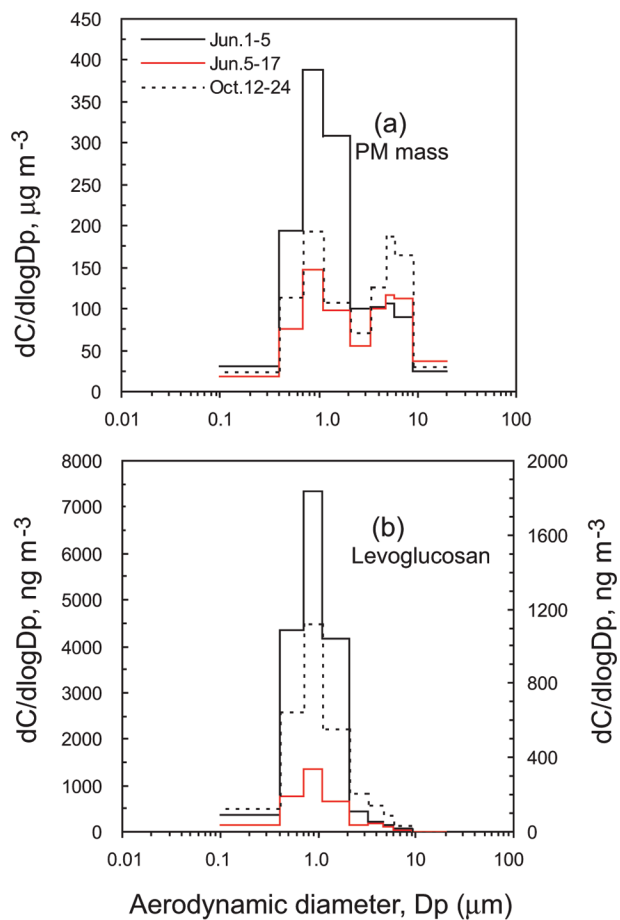


FIGURE 2. Size distributions of the concentrations of (a) aerosol mass and (b) levoglucosan (levoglucosan concentrations from June 1–5 are referred to on the left *y*-axis and those from June 5–17 and Oct. 12–24 are referred to on the right *y*-axis).

between the fine and coarse modes. The GMD ($0.89 \mu\text{m}$, Table 2) of fine particles in the June 1–5 sample was around 10% larger than those of other periods ($0.81 \pm 0.06 \mu\text{m}$ on June 5–17 and $0.77 \pm 0.04 \mu\text{m}$ on Oct. 12–24). Yang et al. (18) reported that particles emitted from biomass burning are larger than those from fossil fuel combustion. Thus the above result suggests the haze sample (i.e., June 1–5 sample) was more influenced by the wheat straw burning. However, the coarse mode GMD ($4.37 \mu\text{m}$) of particles during the haze period was 10–15% smaller than those in the nonhaze periods ($4.88 \pm 0.08 \mu\text{m}$ on June 5–17 and $4.98 \pm 0.15 \mu\text{m}$ on Oct. 12–24), which may be due to the enhanced deposition of the large particles under the lower wind speed conditions during June 1–5 (Table S1). Levoglucosan is evaporated into the air during the biomass burning process and subsequently condensed and/or adsorbed onto pre-existing fine particles whose surface area per units of weight are larger than that of coarse particles. Therefore it centered in fine mode with a maximum at the $0.7\text{--}1.1 \mu\text{m}$ size for all the samples (Figure 2b).

n-Alkanes originated from plant wax and fossil fuel combustion showed a unimodal size distribution for the haze event sample (i.e., June 1–5) and a bimodal size distribution for the nonhaze samples (i.e., June 5–17 and Oct. 12–24) (Figure 3a and b). During the haze event plant wax derived *n*-alkanes showed the second highest concentration in the size $1.1\text{--}2.1 \mu\text{m}$ (Figure 3a), whereas fossil fuel derived *n*-alkanes present the second highest concentration in a smaller size ($0.4\text{--}0.7 \mu\text{m}$) (Figure 3b). Such a size distribution difference between the two types of

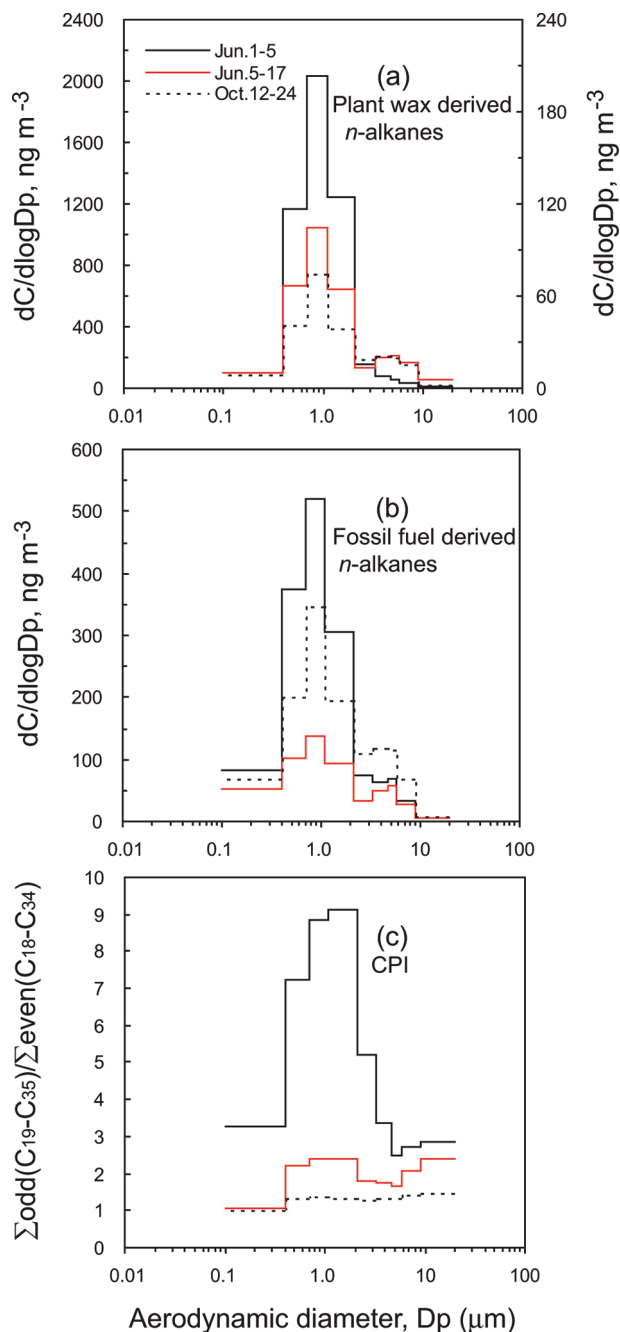


FIGURE 3. Size distributions of (a) plant wax derived *n*-alkanes, (b) fossil fuel derived *n*-alkanes, and (c) CPI of *n*-alkanes (plant wax derived *n*-alkanes are calculated as the excess odd homologues – adjacent even homologues average, and the difference from the total *n*-alkanes is the fossil fuel derived *n*-alkanes (11). Concentrations of plant wax derived *n*-alkanes on June 1–5 are referred to on the left *y*-axis and those during June 5–17 and Oct. 12–24 are referred to on the right *y*-axis).

n-alkanes was not observed for the nonhaze samples, again suggesting aerosols produced by the wheat straw burning are of larger sizes. In addition, the biomass burning derived particles were enriched with hydrophilic species (e.g., K^+ and sugars) and also experienced longer residence time during the transport into the urban area, therefore their hygroscopic growth and/or coagulation were probably enhanced compared to the urban fossil fuel emissions, resulting in the largest fine mode GMDs (19).

Compared with a CPI in each stage for the nonhaze periods, the values were found to be much higher for the June 1–5 sample with a maximum at the range $1.1\text{--}2.1 \mu\text{m}$

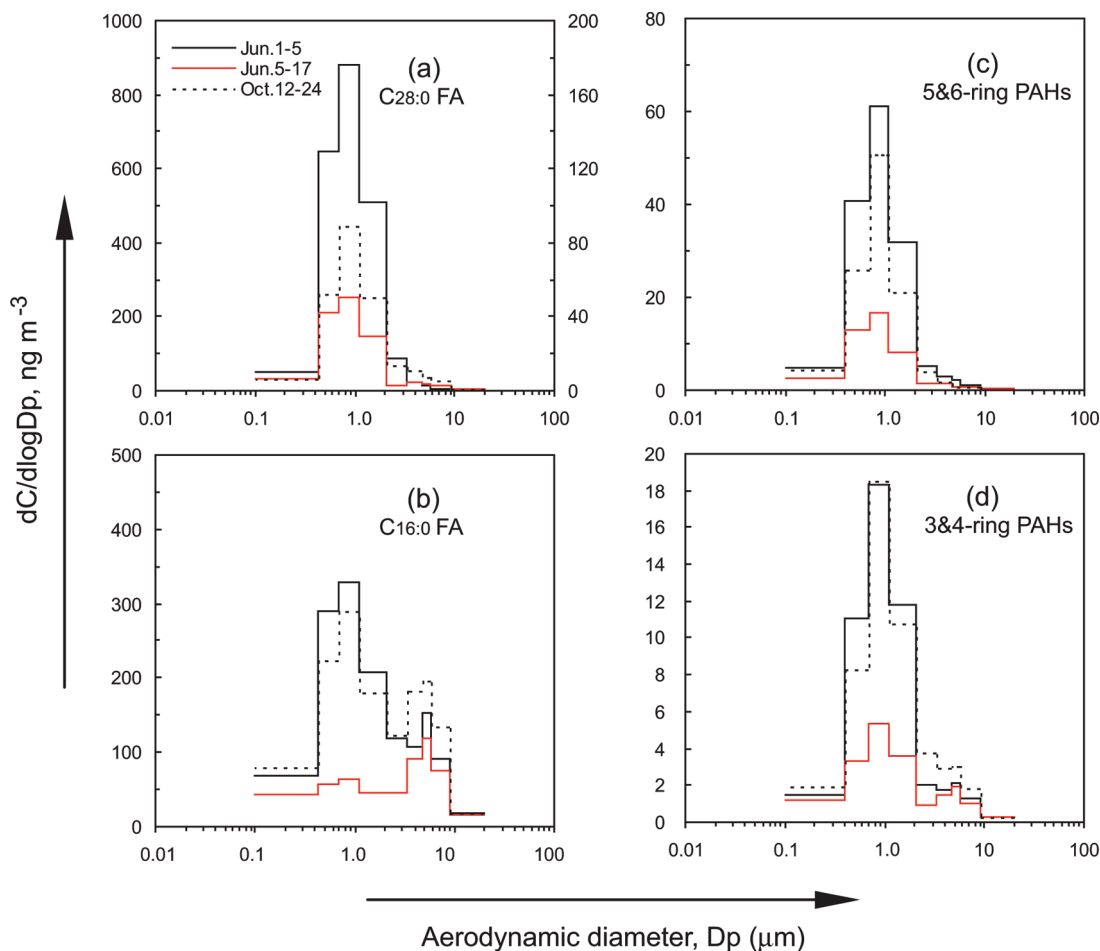


FIGURE 4. Size distributions of (a) $C_{28:0}$ fatty acid (concentrations of FA $C_{28:0}$ on June 1–5 are referred to on the left y -axis and those on June 5–17 and Oct. 12–24 are referred to on the right y -axis), (b) $C_{16:0}$ fatty acid, (c) 5- and 6-ring PAHs, and (d) 3- and 4-ring PAHs.

TABLE 2. Geometric Mean Diameter (GMD, μm)^a of Biomarkers in the Fine and Coarse Mode Particles

	fine mode (<2.1 μm)			coarse mode ($\geq 2.1 \mu\text{m}$)		
	June 1–5 ($n = 1$)	June 5–17 ($n = 3$)	Oct. 12–24 ($n = 3$)	June 1–5 ($n = 1$)	June 5–17 ($n = 3$)	Oct. 12–24 ($n = 3$)
I. PM and levoglucosan						
PM	0.89	0.81 \pm 0.06	0.77 \pm 0.04	4.37	4.88 \pm 0.08	4.98 \pm 0.15
levoglucosan	0.86	0.79 \pm 0.09	0.76 \pm 0.03	3.42	3.79 \pm 0.19	3.50 \pm 0.04
II. n -alkanes						
Σn -alkanes	0.84	0.68 \pm 0.03	0.71 \pm 0.04	3.66	4.44 \pm 0.22	4.15 \pm 0.09
C_{25}	0.76	0.65 \pm 0.04	0.71 \pm 0.06	3.97	4.35 \pm 0.21	3.98 \pm 0.02
C_{31}	0.84	0.76 \pm 0.05	0.76 \pm 0.05	3.54	4.56 \pm 0.35	4.05 \pm 0.17
plant wax	0.87	0.83 \pm 0.08	0.77 \pm 0.06	3.46	4.57 \pm 0.26	4.31 \pm 0.08
fossil fuel	0.73	0.61 \pm 0.02	0.70 \pm 0.04	3.97	4.38 \pm 0.20	4.12 \pm 0.08
III. fatty acids						
Σ FAs	0.81	0.64 \pm 0.05	0.73 \pm 0.02	3.84	4.72 \pm 0.21	4.32 \pm 0.10
$C_{16:0}$	0.69	0.51 \pm 0.08	0.65 \pm 0.01	4.30	4.74 \pm 0.20	4.46 \pm 0.11
$C_{28:0}$	0.84	0.78 \pm 0.08	0.84 \pm 0.04	3.08	4.41 \pm 0.51	3.80 \pm 0.13
IV. PAHs						
Σ PAHs	0.81	0.70 \pm 0.04	0.79 \pm 0.07	3.78	4.30 \pm 0.20	3.72 \pm 0.12
3&4-ring	0.84	0.71 \pm 0.03	0.80 \pm 0.07	4.14	4.54 \pm 0.20	4.05 \pm 0.17
5&6-ring	0.79	0.69 \pm 0.05	0.78 \pm 0.08	3.55	3.86 \pm 0.42	3.05 \pm 0.03

^a GMD: $\log\text{GMD} = (\sum C_i \log D_{p_i}) / \sum C_i$, where C_i is the concentration of compound in size i and D_{p_i} is the geometric mean particle diameter collected on stage i (17).

mainly due to the wheat straw burning emissions (Figure 3c). In contrast, CPI values for the June 5–17 samples showed two maxima at the size ranges of 0.7–2.1 μm and $>9.0 \mu\text{m}$. However, the CPI values in the autumn samples are close to

unity in whole size ranges, suggesting a strong contribution of fossil fuel derived n -alkanes in each of the particle sizes.

3.2.2. Fatty Acids and PAHs. Concentrations of total fatty acids (FA) showed a unimodal size distribution in the June

TABLE 3. Concentrations (ng m⁻³) and Diagnostic Ratios of Hopanes in the Summer Sampling Periods

date	C _{29αβ} ^a	C _{30αβ} ^b	C _{29αβ} /C _{30αβ}	C _{31αβ} S/[S+R] ^c	C _{32αβ} S/[S+R] ^d
June 1–5	3.3	4.4	0.75	0.67	0.55
June 5–17	1.7	2.1	0.79	0.65	0.58
June 1–5/June 5–17	2.0	2.1			

^a C_{29αβ}: 17α(H),21β(H)-30-norhopane. ^b C_{30αβ}: 17α(H),21β(H)-30-hopane. ^c C_{31αβ} S/[S+R]: 17α(H),21β(H)-22S-homohopane/[17α(H),21β(H)-22S-homohopane + 17α(H),21β(H)-22R-homohopane]. ^d C_{32αβ} S/[S+R]: 17α(H),21β(H)-22S-bishomohopane/[17α(H),21β(H)-22S-bishomohopane + 17α(H),21β(H)-22R-bishomohopane].

TABLE 4. Impact of Emissions from Wheat Straw Burning on June 1–5, ng m⁻³

	ambient concentration		impact of wheat straw burning on June 1–5
	June 1–5	June 5–17	
levoglucosan	4030	204	3622
n-alkanes	2152	218	1716
fatty acids	2629	476	1677
PAHs	57	19	19

1–5 sample, compared to the bimodal distributions in non-event samples. Figure 4a showed a C_{28:0} FA peak at 0.7–1.1 μm but with the smallest GMD (0.78 ± 0.08 μm, Table 2) on June 5–17. Figure 4b showed that C_{16:0} FA presented a bimodal distribution peaking at 0.7–1.1 and 4.7–5.8 μm in diameter for all the samples. However, coarse mode of FA C_{16:0} is more abundant for the June 5–17 samples. The GMDs of ΣFA, C_{16:0}, and C_{28:0} during the haze event are 0.81, 0.69, and 0.84 μm in the fine mode, and 3.84, 4.30, and 3.08 μm in the coarse mode, respectively.

Past studies showed that LMW PAHs (≤228 MW) partition to varying extents into the gas phase, while HMW PAHs (≥252) appear almost entirely in solid phase (20). Gas-particle partitioning of pollutants depends on the vapor pressure of each species and the surface area of particles (21). Figure 4c shows that HMW 5- and 6-ring PAHs presented a highest concentration in the 0.7–1.1 μm range, followed by the 0.4–0.7 μm range. In contrast, LMW 3- and 4-ring PAHs showed a similar maximum concentration peak (0.7–1.1 μm) but a large secondary peak in the size range of 1.1–2.1 μm (Figure 4d). The fine mode of GMDs (0.79, 0.69, and 0.78 μm for the June 1–5, June 5–17, and Oct. 12–24 samples, respectively, Table 2) of HMW 5- and 6-ring PAHs are smaller than those (0.84, 0.71, and 0.80 μm for the June 1–5, June 5–17, and Oct. 12–24 samples, respectively) of LWM 3- and 4-ring PAHs. Such a preferential accumulation of LMW PAHs in larger particles, consistent with those observed by Offenberg and Baker (22), could result from the repartitioning of the semivolatile PAHs between the gas and the particle phases with larger accumulation-mode under certain conditions (23, 24). The small peak found for the LMW PAHs at size range of 4.7–5.8 μm during June 5–17 was probably due to adsorption of the semivolatile PAHs onto coarse particles. PAHs in the June 1–5 sample also showed the largest GMD (0.84 μm, Table 2) in the fine mode among the three periods, suggesting enhanced fine particle coagulation and organic repartitioning (19).

3.3. Impact of Organic Aerosols by the Wheat Straw Burning during June 1–5. Hopanes have been used as markers for fossil fuel combustion (11). Molecular compositions of hopanes and concentration ratios (i.e., 2–2.1) of C_{29αβ} and C_{30αβ} between June 1–5 and June 5–17 samples were similar (Table 3). Because there were no significant changes in the meteorological conditions except for the low wind speed on June 1–5, difference in the concentrations of hopanes may be attributed to accumulation effect

for the June 1–5 sample. Therefore, the impact of organic aerosols by wheat straw burning during June 1–5 equals concentrations of organic aerosols during June 1–5 – 2 × concentrations of organic aerosols during June 5–17.

As shown in Table 4, 33–85% of organic aerosols on June 1–5 were contributed by the wheat straw burning depending on compound classes, revealing that the urban air aerosol was significantly influenced by the field biomass burning.

Acknowledgments

This work was financially supported by China Natural Science Foundation (40873083), the Knowledge Innovation Program of Chinese Academy of Sciences (KZCX2-YW-148), and a Grant-in-Aid (19204055) from the Japan Society for the Promotion of Science (JSPS).

Supporting Information Available

Meteorological information during sampling periods and relative abundance of organic compounds in fine (<2.1 μm) and coarse (≥2.1 μm) modes (Table S1 and Figure S1). This material is available free of charge via the Internet at <http://pubs.acs.org>.

Literature Cited

- Menon, S.; Hansen, J.; Nazarenko, L.; Luo, Y. Climate effects of black carbon aerosols in China. *Science* **2002**, *297*, 2250–2253.
- Dockery, D. W.; Pope, C. A.; Xu, X.; Spengler, J. D.; Ware, J. H.; Fay, M. E.; Ferris, B. G., Jr.; Speizer, F. E. An association between air pollution and mortality in six U.S. cities. *N. Engl. J. Med.* **1993**, *329*, 1753–1759.
- Brooke, L.; Seinfeld, J. H. On the hygroscopic behavior of atmospheric organic aerosols. *Ind. Eng. Chem. Res.* **2001**, *40*, 4162–4171.
- Jacobson, M. Z. Strong radiative heating due to the mixing state of black carbon in atmospheric aerosols. *Nature* **2001**, *409*(6821), 695–697.
- Seinfeld, J. H.; Pankow, J. F. Organic atmospheric particulate material. *Annu. Rev. Phys. Chem.* **2003**, *54*, 121–140.
- Dillner, A. M.; Schauer, J. J.; Zhang, Y.; Zeng, L.; Cass, G. R. Size-resolved particulate matter composition in Beijing during pollution and dust events. *J. Geophys. Res.* **2006**, *111*, D05203; doi: 10.1029/2005JD006400.
- Liu, J. G.; Diamond, J. China's environment in a globalizing world: How China and the rest of the world affect each other. *Nature* **2005**, *435*, 1179–1186.
- Li, X.; Wang, S.; Duan, L.; Hao, J.; Li, C.; Chen, Y.; Yang, L. Particulate and trace gas emissions from open burning of wheat straw and corn stover in China. *Environ. Sci. Technol.* **2007**, *41*, 6052–6058.
- Wang, G. H.; Kawamura, K. Molecular characteristics of urban organic aerosols from Nanjing: A case study of a mega-city in China. *Environ. Sci. Technol.* **2005**, *39*, 7430–7438.
- Simoneit, B. R. T.; Sheng, G.; Chen, X.; Fu, J.; Zhang, J.; Xu, Y. Molecular markers of extractable organic matter in aerosols from urban areas of China. *Atmos. Environ., Part A* **1991**, *25*(10), 2111–2129.
- Simoneit, B. R. T.; Kobayashi, M.; Mochida, M.; Kawamura, K.; Lee, M.; Lim, H. J.; Turpin, B. J.; Komazaki, Y. Composition and major sources of organic compounds of aerosol particulate matter sampled during the ACE-Asia campaign. *J. Geophys. Res.-Atmos.* **2004**, *109*, D19S10; doi: 10.1029/2004JD004598.

- (12) Simoneit, B. R. T.; Elias, V. O. Detecting organic tracers from biomass burning in the atmosphere. *Mar. Pollut. Bull.* **2001**, *42* (10), 805–810.
- (13) Deswarte, F. E. I.; Clark, J. H.; Hardy, J. J. E.; Rose, P. M. The fractionation of valuable wax products from wheat straw using CO₂. *Green Chem.* **2006**, *8*, 39–42.
- (14) Grimmer, G.; Jacob, J.; Noujack, K. W. Profile of the polycyclic aromatic hydrocarbons from lubricating oils. Inventory by GC/MS-PAH in environmental materials, Part 1. *Fresenius' J. Anal. Chem.* **1983**, *314*, 13–19.
- (15) Ohura, T.; Amagai, T.; Fusaya, M.; Matsushita, H. Polycyclic aromatic hydrocarbons in indoor and outdoor environments and factors affecting their concentrations. *Environ. Sci. Technol.* **2004**, *38* (1), 77–83.
- (16) Vaeck, L. V.; Cauwenberghe, K. A. V. Characteristic parameters of particle size distributions of primary organic constituents of ambient aerosols. *Environ. Sci. Technol.* **1985**, *19*, 707–716.
- (17) Hinds, W. C. *Aerosol Technology: Properties, Behavior, and Measurement of Airborne Particles*; John Wiley & Sons: New York, 1999.
- (18) Yang, H.-H.; Tsai, C.-H.; Chao, M.-R.; Sua, Y.-L.; Chiena, S.-M. Source identification and size distribution of atmospheric polycyclic aromatic hydrocarbons during rice straw burning period. *Atmos. Environ.* **2006**, *40*, 1266–1274.
- (19) Herner, J. D.; Ying, Q.; Aw, J.; Gao, O.; Chang, D. P. Y.; Kleeman, M. J. Dominant mechanism that shape the airborne particle size and composition distribution in central California. *Aerosol Sci. Technol.* **2006**, *40*, 827–844.
- (20) Yamasaki, H.; Kuwata, K.; Miyamoto, H. Effects of ambient temperature on aspects of airborne polycyclic aromatic hydrocarbons. *Environ. Sci. Technol.* **1982**, *16*, 189–194.
- (21) Finlayson-Pitts, B. J.; Pitts, J. N., Jr. *Chemistry of the Upper and Lower Atmosphere*; Academic Press: San Diego, CA, 2000.
- (22) Offenberg, J. H.; Baker, J. E. Aerosol size distributions of polycyclic aromatic hydrocarbons in urban and over-water atmospheres. *Environ. Sci. Technol.* **1999**, *33*, 3324–3331.
- (23) Kleeman, M. J.; Riddle, S. G.; Jakober, C. A. Size distribution of particle-phase molecular markers during a severe winter pollution episode. *Environ. Sci. Technol.* **2008**, *42*, 6469–6475.
- (24) Venkataraman, C.; Lyons, J. M.; Friedlander, S. K. Size distribution of polycyclic aromatic hydrocarbons and elemental carbon. 2. Ambient measurements and effects of atmospheric processes. *Environ. Sci. Technol.* **1994**, *28*, 563–572.
- (25) Kavouras, I. G.; Stephanou, E. G. Particle size distribution of organic primary and secondary aerosol constituents in urban, background marine, and forest atmosphere. *J. Geophys. Res.-Atmos.* **2002**, *107* (D8), 4069; doi: 10.1029/2000JD000278.

ES803086G